INLAND WATERS
2018, VOL. 8, NO. 3, 381–398
https://doi.org/10.1080/20442041.2018.1505372

Ice cover and thermal regime in a dimictic seepage lake under climate change

David P. Hamilton [a], Madeline R. Magee [b], Chin H. Wu [b] and Timothy K. Kratz [c]

[a]Australian Rivers Institute, Griffith University, Brisbane, Australia; [b]Department of Civil and Environmental Engineering, University of Wisconsin, WI, USA; [c]Trout Lake Station, Center for Limnology, University of Wisconsin-Madison, Boulder Junction, WI, USA

ABSTRACT

Changes in water temperature and ice cover are important for controlling the biogeochemical and food-web processes of dimictic lakes in temperate regions. To investigate these changes, we applied a 1-dimensional hydrodynamic lake-ice model to Crystal Lake, a 20 m deep, dimictic seepage lake in northern Wisconsin, USA, to a period of 23 years (1989–2011). The model, DYRESM-WQ-I, incorporates the evolution of blue ice, white ice, and snow cover; time-varying ice and snow albedo; and 2-way coupling across the ice–water interface by incorporating components of previous ice models embedded in the hydrodynamic component of the DYRESM-WQ model. A new element of the current model is time-varying sediment heat fluxes, important to under-ice water temperatures in shallow lakes. Simulations closely reproduce the observed annual stratification regime and ice phenology with standard errors in temperature of 0.7 °C; total difference of 10–20% in ice thickness compared with measured values; and standard errors of 0.9 d for ice-on and 1.55 d for ice-off. Under a likely future climate scenario involving changes in air temperature forecasted to occur by the middle of this century (2055), results suggest an average reduction in mean ice cover thickness of about 0.18 m and an increase in surface mixed-layer temperature of up to 3.5 °C over summer. In addition, water levels decreased by 5.1 m over the simulation period, mostly in response to greater evaporation from higher surface water temperature in summer. The results have important implications for seepage lakes in temperate regions, where projected changes in precipitation with climate warming will not compensate for increased evaporation from the lake surface and the likely alteration in groundwater flows.

ARTICLE HISTORY
Received 25 December 2015
Accepted 16 April 2018

KEYWORDS
climate change; dimictic lakes; ice cover; seepage lakes; thermal regime; water levels

Introduction

The thermal regime, ice cover phenology, and interrelated hydrology and biogeochemistry of dimictic lakes are sensitive to anthropogenically mediated variations in climate (Magnuson et al. 1997, Weyhenmeyer et al. 1999, Fang and Stefan 2009). This sensitivity is related to changes in water temperature (Robertson and Ragotzkie 1990, Assel and Robertson 1995, Peeters et al. 2002) and duration and thickness of ice cover (Robertson et al. 1992, Assel and Robertson 1995, Jensen et al. 2007). Hutchinson (1975) showed that the temperature stratification regime of dimictic lakes is critical in controlling the transport and distribution of dissolved and particulate constituents of the water. Ice cover plays an important role in lake–atmosphere heat balances because it greatly increases the surface albedo, which reduces shortwave radiation absorption by the water, affects evaporation, and changes the effect of wind on mixing. Although temperature gradients under ice are generally small (Ellis et al. 1991, Bengtsson et al. 1996), the dynamics of the thermal regime under ice and changes to that regime as a result of climate warming can affect biogeochemical processes and complex food-web cycles in lakes (Carpenter et al. 1992, Schindler et al. 1992, Agbeti and Smol 1995, De Stasio et al. 1996, Stefan et al. 1996, Magnuson et al. 1997, Melack et al. 1997). In view of these consequences, examining the impacts of climate change on both thermal regime and ice cover in dimictic lakes is crucial.

Few applications of hydrodynamic models resolve lake thermodynamics in combination with formation and ablation of ice cover, despite the importance of ice cover for continuous year-to-year simulations of lakes in colder climates. Models that do not include ice cover are restricted to simulation of only the open-water period. An application of DYRESMI (Patterson and Hamblin 1988) incorporating a sea-ice model (Maykut and Untersteiner 1971) coupled to a lake mixing model, DYRESM (Imberger and Patterson 1981), was used to determine water temperature beneath ice and predict the accretion and ablation of ice at the ice–water interface. Another model, MINLAKE96, simulates

CONTACT Chin Wu chinwu@engr.wisc.edu

water temperature, ice cover, and snow depth (Gu and Stefan 1990, Fang et al. 1996, Fang and Stefan 2009) at a daily time interval. Neither model simulates snow ice formation due to surface flooding, however, which may be especially important to heat fluxes to the water column and resulting winter temperature and circulation dynamics in mid-latitude lakes (Rogers et al. 1995, Kirillin et al. 2012, Oveisy and Boegman 2014).

Ashton (1986) found that formation of snow ice from the refreeze of slush (melted snow) is common in ice-covered lakes. Snow ice has distinct optical and radiative properties compared with blue ice (or congelation ice) that forms from freezing water associated with precipitation. The MyLake model, developed by Saloranta and Andersen (2007), does include snow ice but assumes it has the same properties as blue ice. Other models, such as LIMNOS (Vavrus et al. 1996), a model developed by Liston and Hall (1995), and the General Lake Model (Bueche et al. 2017) are capable of simulating snow ice formation, but no validation data have been provided owing to a lack of separation of blue ice and snow ice thickness. A modification of DYRESMI by Rogers et al. (1995) included formation of snow ice and added several other features, such as snowmelt due to rain, variability in snow density, and snow albedo and conductivity. This modified DYRESMI model yields better predictions of ice/snow cover and under-ice water temperature than those of an earlier DYRESMI version (Imberger and Patterson 1981), but the model removed vertically resolved temperature variations through the water column to reduce computational times. Oveisy and Boegman (2014) improved the Mixed Lake with Ice (MLI) model of Rogers et al. (1995) by incorporating 2-way coupling between water and ice. Nevertheless, sediment heat flux is considered constant rather than temporally variable, which is important to accurately simulate water temperatures (Fang and Stefan 1996a, 1996b). Currently, a model that incorporates temporal heat exchanges between both ice and water, and sediment and water, is still needed to resolve lake thermodynamics under climate change.

Quantitative assessments on the effects of climate change on physical lake processes, particularly in small- and medium-sized lakes, are limited by inadequate spatial resolution in global climate models (GCMs). Considerable effort has been devoted to examining trends and variations of climate in Wisconsin, USA (Scheller and Mladenoff 2005, Serbin and Kucharik 2009, Kucharik et al. 2010). One of the key outcomes of this effort is the Wisconsin Initiative on Climate Change Impacts (WICCI; http://www.wicci.wisc.edu/index.php), which produced a regional-scale, daily historical climate dataset and climate projection by downscaling the ensemble of outputs of 14 different GCMs to a 0.1° latitude × 0.1° longitude grid over Wisconsin. These downscaled data from WICCI are highly suitable to provide a representative projected future climate at a regional scale for predicting future climate impacts on Wisconsin lakes.

Our purpose was to address the long-term dynamics of thermal regime and ice phenology in a dimictic seepage lake in response to a projected climate scenario. We incorporated previous ice and snow models into the existing DYRESM-WQ model (Hamilton and Schladow 1997) and additionally included temporally variable sediment heat flux. This revised model, DYRESM-WQ-I, was then employed to run a long-term (i.e., 23 yr) simulation on a dimictic seepage lake with validation using measured water temperatures and an extensive dataset for blue- and white-ice thickness and snow thickness. Furthermore, future climate scenarios were performed using the downscaled climate projection data from WICCI. Results of climate change effects on lakes related to ice duration, thermal regime, and resultant impacts on the biota are discussed with a particular focus on the hydrological factors (e.g., water levels) that may affect these assessments.

Study site

Crystal Lake (46°01′N, 89°37′W) is a small (36 700 m^2) lake located in the forested Northern Highland Lake District of northern Wisconsin, USA (Fig. 1). The lake is dimictic and oligotrophic, with a maximum depth of 20 m, a mean depth of 10.4 m, and high water clarity, resulting in a relatively deep thermocline in summer. In a typical year, Crystal Lake freezes over in late

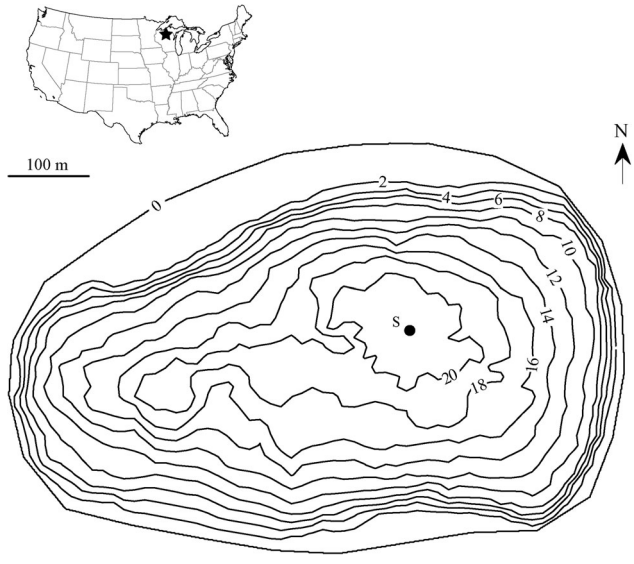

Figure 1. Location and bathymetry (m) of Crystal Lake, WI, with sampling station denoted by S.

Table 1. Timing and duration of ice cover in Crystal Lake based on measurements during 1981–2011. The years corresponding to the upper and lower limits of each ice parameter are in parentheses.

Ice cover index	Mean ($n = 31$)	SD	Range
Ice-on (date)	1 Dec	8.6	17 Nov 1986 to 24 Dec 2001
Ice-off (date)	20 Apr	9.65	29 Mar 2010 to 11 May 1996
Duration (day)	140.4	14.7	106 (1999–2000) – 171 (1995–1996)

November (ice-on) and ice breaks up in mid-April (ice-off; Table 1). The average ice duration is about 3–4 months. Ice data for the lake are available at the North Temperate Lakes Long Term Ecological Research (NTL-LTER) Program website (http://lter.limnology.wisc.edu). The timing and variation in formation and break-up of ice in Crystal Lake are based on data from 1981 to 2011 (Table 1).

Geologically, the area is dominated by a sandy outwash plain consisting of 30–50 m of unconsolidated sand and coarser till overlying Precambrian igneous bedrock. The predominant soils are thin forest soils with high organic content in the uppermost horizon. The site is representative of the glacial lake districts common to the upper Midwest and Canada. Crystal Lake is positioned at an elevation of 502 m a.s.l. near the groundwater divide in the Trout Lake basin. Groundwater inflow contributes a small fraction (~5%) of the total annual water input, occurring predominantly in the littoral zone (Kenoyer and Anderson 1989). The lake is classified as seepage, with no stream inlets or outlets; the hydrological budget indicates it is precipitation-dominated, and evaporation from the lake surface is the major loss term (Webster et al. 2006). Ice cover limits the duration of evaporation, with changes in ice cover impacting the total evaporation, thus influencing lake levels.

Methods

DYRESM-WQ-I model

A 1-dimensional (1D) representation serves adequately to resolve the vertical thermal structure for small- to medium-sized lakes (Imberger and Patterson 1990). In this study, we added a 3-component ice and snow model based on Rogers et al. (1995) to the existing 1D hydrodynamic model, DYRESM-WQ (Hamilton and Schladow 1997), incorporated variable ice and snow albedo based on Vavrus et al. (1996), and included a new component of time-varying sediment heat flux. The DYRESM-WQ-I model has been employed by Magee et al. (2016) and Magee and Wu (2017a, 2017b) to reveal shifts of lake thermal variables and ice cover for 3 southern Wisconsin Lakes in response to changing climate.

Hydrodynamic model

The hydrodynamic portion of the model was that of DYRESM-WQ, which takes fixed data for lake geometry, bathymetry, and initial conditions and uses meteorological data, inflow volume and composition, and outflow volume to resolve the vertical distribution of temperature and salinity as a series of horizontally homogeneous layers. The number and size of the layers were variable depending on resolution required to accurately reproduce the vertical density profile. Model output included temperature at each vertical layer of the model, water level, and heat fluxes at the lake surface for each day of simulation. Note that the DYRESM-WQ model redistributes daily shortwave radiation input within the model as a sinusoid over the photoperiod, based on lake latitude and time of year (Hamilton and Schladow 1997). Water levels were calculated by determining the volume of water in the lake at each time step after additions from direct precipitation and inflow and subtractions from evaporation and outflow, and then distributing the water volume for each layer based on lake bathymetry input. The vertical transfer of heat in the water column beneath the ice was regulated by a dynamically assigned thermal diffusion coefficient. The formulation used in DYRESM-WQ-I produced diffusivities within the range of measurements by Ellis et al. (1991), which were 1–3 times greater than molecular diffusivity. A dynamic light extinction coefficient was determined from an assigned background level and from concentrations of appropriate light attenuating constituents of water (e.g., chlorophyll *a*). Other than fitting groundwater inflow and outflow so that simulated water levels matched observed values, the model required no lake-specific calibration.

Sediment heat flux

Sediment heat transfers are important to water temperatures beneath ice cover (Hutchinson 1975, Ellis et al. 1991, Tsay et al. 1992). We represented this process by estimating the areal rate of heat transfer from the sediments to the water column by:

$$q_{sed} = K_{sed} \frac{\mathrm{d}T}{\mathrm{d}z}, \tag{1}$$

where K_{sed} is the sediment conductivity and $\mathrm{d}T/\mathrm{d}z$ (z was defined as positive upward) is the temperature gradient across the sediment–water interface:

$$\frac{\mathrm{d}T}{\mathrm{d}z} \approx \frac{T_s - T_w}{z_{sed}}, \tag{2}$$

where T_s is the sediment temperature, T_w is the water temperature adjacent to the sediment surface, calculated by DYRESM-WQ-I at hourly time steps, and z_{sed} is the

distance beneath the water at which sediment temperature would increase from T_s to T_w if the variation were linear. Birge et al. (1927) found that sediment temperatures at 5 m varied little throughout the year in Lake Mendota. Here we set z_{sed} to be 5 m and fit data from Birge et al. (1927) to describe the temporal variation of T_s:

$$T_s = 9.7 + 2.7\sin\left[\frac{2\pi(D-151)}{TD}\right], \quad (3)$$

where D is the number of days from the start of the year and TD is the total number of days for the year of interest (i.e., 365 or 366). The temporal and vertical variations in sediment heat fluxes are estimated from the above formulae, in close agreement with previous estimates by Scott (1964). To reduce computational cost, this model represents a simplified version of that presented by Fang and Stefan (1996a), which simulated both ice cover and the water temperature under the ice.

Ice–snow model

We implemented an ice and snow model based on the earlier MLI model by Rogers et al. (1995). The ice-snow model is run on a 1 h time step; however, ice compaction, snowfall, and rainfall components of the model are run at a daily time step because variation for ice processes is longer than the time scale of short-term, hourly meteorological variability. For brevity, only fundamental equations and those that differ from Rogers et al. (1995) are shown. To solve the heat transfer equation, the ice model used a quasi-steady state assumption that the time scale for heat conduction through the ice is short relative to the time scale of meteorological forcing (Patterson and Hamblin 1988, Rogers et al. 1995). A Stefan number <0.1 (defined as the ratio of sensible heat to latent heat) can validate this assumption (Hill and Kucera 1983). Based on Rogers et al. (1995), if air temperature is less than −15.9 °C, then the Stefan number is <0.1, and the assumption is valid. The steady state conduction equations, which allocate shortwave radiation into 2 components, a visible ($A_1 = 70\%$) and a near-infrared ($A_2 = 30\%$) spectral band, are used with a 3-component ice model that includes blue ice, snow ice, and snow (adapted from equation 1 in Rogers et al. 1995; Fig. 2). Snow ice is generated in response to flooding, when the mass of snow that can be supported by the ice cover is exceeded (see equation 13 in Rogers et al. 1995). By assigning appropriate boundary conditions to the interfaces and solving the quasi-steady state of heat transfer numerically, the upward conductive heat flux between the ice or snow cover and the atmosphere, q_0, can be determined. The estimation of q_0 involved the application of an empirical equation (Ashton 1986) to estimate snow conductivity (K_s) from its density, where the density of snow was determined (Fig. 3).

The uppermost solid layer (ice or snow) was adjusted in thickness at the end of each 1 h model time step, according to the balance of heat budget:

$$\begin{aligned} q_0(T_0) + H(T_0) &= 0 \qquad T_0 < T_m \\ &= -\rho L \frac{\mathrm{d}h}{\mathrm{d}t} \qquad T_0 = T_m \end{aligned}, \quad (4)$$

where L is the latent heat of fusion (see physical constants, Table 2), h is the height of the upper snow or ice layer, t is time, ρ is the density of the snow or ice determined from the surface medium properties, T_0 is the temperature at the solid surface, T_m is the melt-water temperature (0 °C), and $H(T_0)$ is the net incoming heat flux, given by:

$$H(T_0) = R_{li} - R_{lo}(T_0) + Q_c(T_0) + Q_e(T_0) + Q_r(T_0), \quad (5)$$

where and R_{li} and R_{lo} are incoming and outgoing longwave radiation, Q_c and Q_e are sensible and evaporative heat fluxes between the solid boundary and the atmosphere, and Q_r is the heat flux due to rainfall. These heat fluxes were derived from standard bulk aerodynamic formulae in DYRESM-WQ (Hamilton and

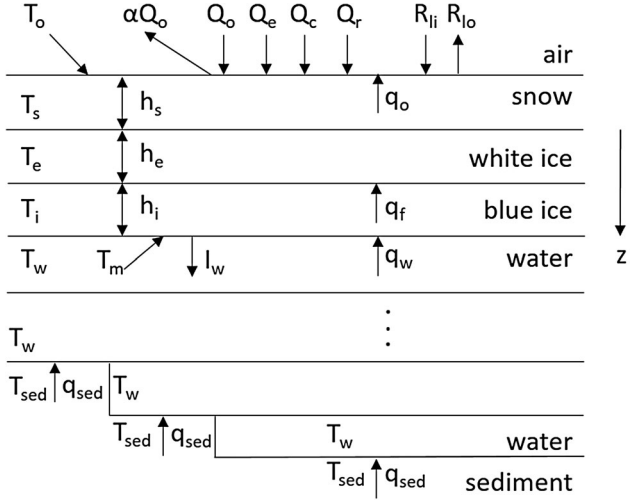

Figure 2. Schematic showing heat fluxes in ice/snow model and between the water and sediment. Q is surface heat flux (o = shortwave, e = evaporative, c = sensible, r = rainfall), I is shortwave heat flux (o = immediately below water surface, w = penetrating to immediate lower water layer), R is longwave radiation (li = incoming, lo = outgoing), q is heat flux between layers (o = ice or snow–atmosphere, f = ice–water, w = water–ice, sed = sediment–water), T is temperature (o = ice or snow–atmosphere boundary, s = snow, e = white ice, i = blue ice, w = water, sed = sediment, m = melt-water), z is elevation, and α is albedo.

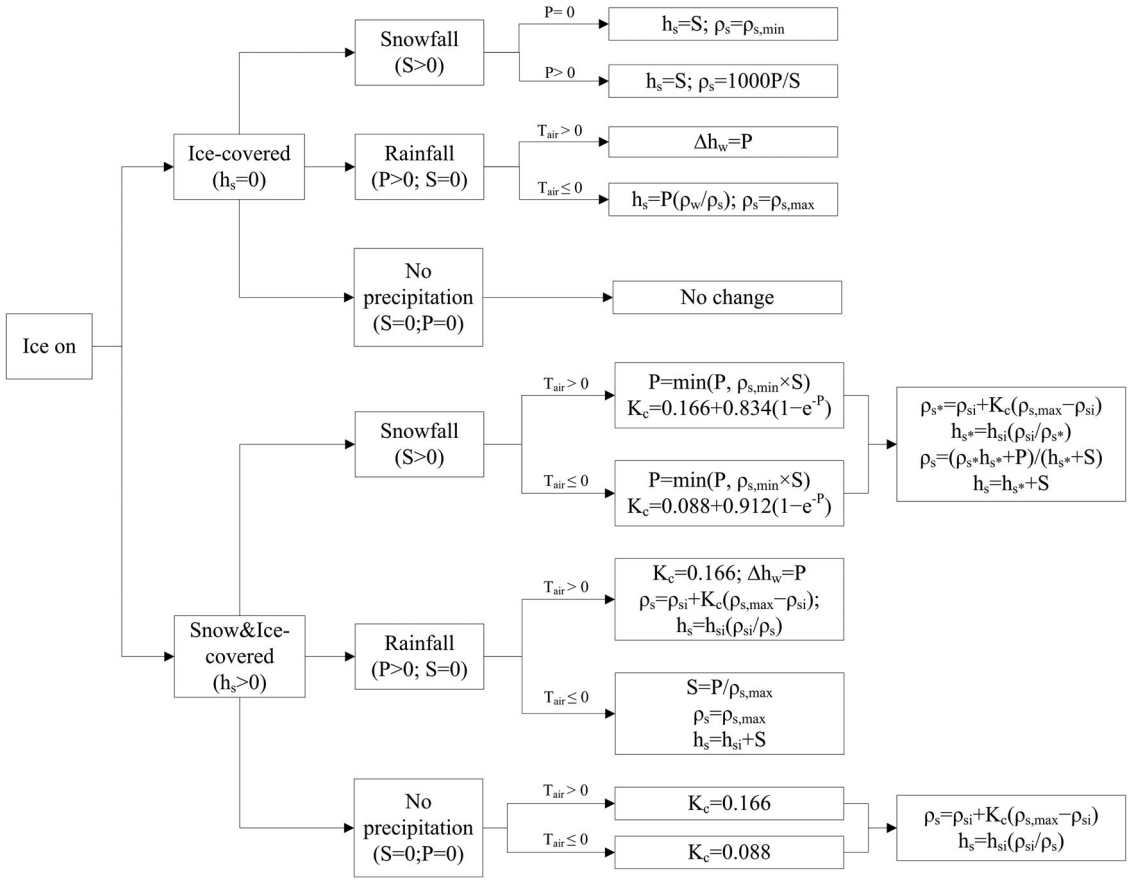

Figure 3. Decision tree to update ice cover, snow cover, and water depth according to snow compaction, rainfall (P), and snowfall (S) on each day, and depth of snow cover (h_{si}) and snow density (ρ_{si}) for the previous day; h_{s*} and ρ_{s*} represent depth of snow cover and snow density, respectively, from compaction of snow before snowfall occurs. Refer to Table 2 for definitions of other variables.

Schladow 1997), with modification for determination of vapor pressure over ice or snow (Gill 1982) and the addition of Q_r (Rogers et al. 1995). T_0 was determined using a bilinear iteration until surface heat fluxes were balanced (i.e., $q_0(T_0) = -H(T_0)$) and T_0 was stable (±0.001 °C). In the presence of ice (or snow) cover, surface temperature $T_0 > T_m$ indicates that energy is available for melting. The amount of energy for melting is calculated by setting $T_0 = T_m$ to determine the reduced thickness of snow or ice.

Accretion or ablation of ice was determined through the heat flux at the ice–water interface, q_f. Solving for heat conduction through ice yields:

$$q_f = q_0 - A_1 I_0\{1 - \exp(-\lambda_{s1}h_s - \lambda_{e1}h_e - \lambda_{i1}h_i)\} - A_2 I_0\{1 - \exp(-\lambda_{s2}h_s - \lambda_{e2}h_e - \lambda_{i2}h_i)\} - Q_{si}h_s, \quad (6)$$

where I_0 is the shortwave radiation penetrating the surface, λ and h are the light attenuation coefficient and thickness of the ice and snow components, respectively, designated with subscripts s, i, and e for snow, blue ice, and snow ice, respectively; Q_{si} is a volumetric heat flux for formation of snow ice (given in equation 14 in Rogers et al. 1995), and subscripts 1 and 2 refer to radiation in the visible (1) and near-infrared spectra (2) bands. In this study, we fixed the ice and snow light attenuation coefficients to the same values as those given by Rogers et al. (1995), noting the close agreement to measured values for our study lake.

Reflection of shortwave radiation from the ice or snow surface is a function of surface temperature and ice and snow thickness (Table 1; Vavrus et al. 1996) based on data derived from Scott (1964) for lakes in the Madison, Wisconsin, area and measurements of sea ice in the central Arctic by Maykut (1982). Ice albedo is shown in equation 7, and snow albedo is provided in equation 8:

Ice albedo

$$\begin{cases} h_i > 0.5\,m \rightarrow \begin{cases} \alpha_i = 0.6 & T_i \le -5\,^\circ C \\ \alpha_i = 0.44 - 0.032T_i & -5\,^\circ C < T_i < 0\,^\circ C \\ \alpha_i = 0.44 & T_i = 0\,^\circ C \end{cases} \\ h_i \le 0.5\,m \rightarrow \alpha_i = 0.08 + 0.44h_i^{0.28} \end{cases}; \quad (7)$$

Table 2. Values of physical constants and parameters used in the ice model. Sources of data were (1) Rogers et al. (1995); (2) measured data for Crystal Lake, (DPH, pers. comm.); (3) Patterson and Hamblin (1988); (4) Vavrus et al. (1996); (5) equations presented in this study; (6) parameters taken to be physical constants; and (7) Ashton (1986).

Parameter	Description	Value	Units	Source
λ_{e1}	Waveband 1, snow ice light extinction	3.8	m^{-1}	1, 2
λ_{e2}	Waveband 2, snow ice light extinction	20	m^{-1}	1, 3
λ_{i1}	Waveband 1, blue ice light extinction	1.5	m^{-1}	1, 2, 3
λ_{i2}	Waveband 2, blue ice light extinction	20	m^{-1}	1, 3
λ_{s1}	Waveband 1, snow light extinction	6	m^{-1}	1, 2, 3
λ_{s2}	Waveband 2, snow light extinction	20	m^{-1}	1, 3
Δz	Distance of heat transfer, ice-water	0.039	m	4
ρ_e	Density, snow ice	890	kg m^{-3}	1
ρ_i	Density, blue ice	917	kg m^{-3}	1, 3
ρ_s	Density, snow	variable	kg m^{-3}	5
c_{pi}	Heat capacity, ice	2.1	kJ kg^{-1} K^{-1}	6
c_{pw}	Heat capacity, water	4.2	kJ kg^{-1} K^{-1}	6
K_c	Compaction coefficient	variable	—	1, 5
K_e	Thermal conductivity, snow ice	2.0	W m^{-1} K^{-1}	1
K_i	Thermal conductivity, blue ice	2.3	W m^{-1} K^{-1}	1, 3
K_s	Thermal conductivity, snow	variable	W m^{-1} K^{-1}	7
K_{sed}	Thermal conductivity, sediment	1.2	W m^{-1} K^{-1}	1
K_w	Thermal conductivity, water	0.57	W m^{-1} K^{-1}	1, 3
L	Latent heat of fusion	334	kJ kg^{-1}	6
T	Daily mean air temperature	variable	°C	—

Snow albedo

$$\begin{cases} \alpha_s = 0.7 & T_i \le -5^\circ C \\ \alpha_s = 0.50 - 0.04 T_s & -5^\circ C < T_i < 0^\circ C \\ \alpha_s = 0.50 & T_i = 0^\circ C \\ \alpha_s = \alpha_s(T_s) - \left(\dfrac{0.1 - h_s}{0.1}\right)[\alpha_s(T_s) - \alpha_i(T_i, h_i)], & h_s \le 0.1\, m \end{cases}; \tag{8}$$

Vavrus et al. (1996) previously determined that this albedo variable is critical to correctly capturing heat fluxes at the ice/snow–air interface and at the ice–water interface because it directly influences penetrative solar radiation through the ice slab. Additionally, the positive feedback involving decreased albedo and increased solar penetration through the ice layer is critical to accurately capturing the rapid decay phase of ice cover during spring melt (Vavrus et al. 1996). Similarly, Oveisy and Boegman (2014) found that variable ice and snow albedo more accurately simulated ice and snow cover thickness compared to constant ice and snow albedo on both Harmon Lake and Eagle Lake in Canada.

The imbalance between q_f and the heat flux from the water to the ice, q_w, gives the rate of change of ice thickness at the interface with water:

$$\frac{dh_i}{dt} = \frac{q_f - q_w}{\rho_i L}, \tag{9}$$

where ρ_i is the density of blue ice and q_w is given by a finite difference approximation of the conductive heat flux from water to ice:

$$q_w = -K_w \frac{\Delta T}{\Delta z}, \tag{10}$$

where K_w is thermal conductivity, and ΔT is the temperature difference between the surface water and the bottom of the ice across an assigned depth Δz. We adopted a value for Δz of 0.5 m based on the reasoning given in Rogers et al. (1995) and the vertical resolution in our hydrodynamic model (0.125–1.5 m). The method employed in this model is not the only method applied throughout the literature, and a wide variation in techniques and values is used to determine the basal heat flux immediately beneath the ice pack (Harvey 1990).

We used a decision tree to update ice cover, snow cover, and water depth in the model (Fig. 3). The ice cover equations were applied when water temperature first dropped below 0 °C. The ice thickness was set to its minimum value of 0.05 m, as suggested by Patterson and Hamblin (1988) and Vavrus et al. (1996). The need for a minimum ice thickness relates primarily to horizontal variability of ice cover during the formation and closure periods. The ice cover equations were discontinued, and open-water conditions were restored in the model when the thermodynamic balance first produced ice thickness <0.05 m. The effects of snowfall, rainfall, and compaction of snow were described through a choice of one of several options, depending on the air temperature and whether ice or snow is the upper boundary (Fig. 3). Density of fresh snowfall on ice was assigned the minimum snow density (ρ_{min} = 50 kg m^{-3}) while density of snow and precipitation on ice was calculated as:

$$\rho_s = \frac{1000 * P}{S}, \tag{11}$$

where ρ_s is the density of snow on ice, P is rainfall depth, and S is measured snowfall, with any values exceeding the assigned maximum snow density ($\rho_{s,max}$ = 300 kg m^{-3}) truncated to the upper limit. The snow compaction model was based on the exponential decay formula of McKay (1968), with selection of snow compaction parameters based on air temperature (Rogers

et al. 1995) as well as on rainfall or snowfall (Fig. 3). The approach of snow compaction used by Rogers et al. (1995) was to set the residual snow density to its maximum value when fresh snowfall occurred. Rogers et al. (1995) found that inaccuracies in snow compaction resulted in underprediction of snow thickness because of increases in snow density that are too rapid under only light snowfall. To resolve this issue, we used a gradual approach to increasing snow compaction that calculates intermediate snow density and height of the residual snow before snowfall occurs, and then calculates the new snow density and height as a function of the residual snow and the fresh snowfall:

$$\rho_{s*} = \rho_{si} + K_c(\rho_{s,\max} - \rho_{si}); \tag{12}$$

$$h_{s*} = h_{si}\left(\frac{\rho_{si}}{\rho_{s*}}\right); \tag{13}$$

$$\rho_s = \frac{(\rho_{s*}h_{s*} + P)}{h_{s*} + S}; \tag{14}$$

$$h_s = h_{s*} + S, \tag{15}$$

where ρ_{s^*} and h_{s^*} represent snow density and depth of snow cover, respectively, from compaction of snow before snowfall occurs; ρ_{si} and h_{si} are snow density and height for the previous day; $\rho_{s,max}$ is the assigned maximum snow density (300 kg m^{-3}); P is the equivalent water height; and S is the snowfall for each day.

Data preparation

A broad suite of physical, chemical, and biological data has been collected routinely in Crystal Lake since 1981 as part of the North Temperate Lakes LTER project (Magnuson et al. 2006). These data included temperature profiles taken at 1 m intervals at a central station corresponding to the deepest part of the lake, thickness of ice cover differentiated into snow ice and blue ice, and snow depth averaged for 10 measurements randomly chosen within 20 m of the sampling location. Measurements were made at 2-week intervals during the open-water season and at ~5-week intervals during periods of ice cover. Photosynthetically active radiation was measured above the surface and at 1 m intervals through the water column, and, measurements were also made during ice cover immediately below the ice. These data were used to determine a light extinction coefficient assuming that light is attenuated exponentially according to Beer's Law. The above physical data were used to assign initial conditions for model simulations and to validate the model results.

Crystal Lake is a precipitation-dominated lake, with groundwater contributing ~5% of the total annual water input to the lake and negligible overland flow and other inputs. Using both measurements and model simulations, Anderson and Cheng (1993) found that groundwater inflows tended to be somewhat transient and inflows were negligible during a period of drought (1989–1991). Based on these observations, we used the following methodology to develop model input data for total daily groundwater inflows and outflows. A water balance for the lake spanning the drought during 1989–1991 was used to derive the groundwater outflow as the residual unknown term; the other terms included evaporation, rainfall, and water level. The total groundwater outflow was then distributed daily for this period by weighting the outflow according to the difference in level between the lake and the surrounding aquifer, the levels of which were closely related. This approach was extended to account for the variation in water level that occurred over the remainder of the 23-year simulation period, with groundwater inflows then estimated as the residual term in a water balance that includes groundwater outflow. Groundwater temperature was taken from routine measurements of wells adjacent to the lake (Department of Natural Resources, WI). Lake water from Crystal Lake and groundwater from surrounding wells both had notably low conductivity, so salinity was assumed to be zero.

Meteorological data inputs to the model were taken from 1989–2011 records at Minocqua Dam and Noble F. Lee Municipal Airport at Woodruff, both located about 15 km southwest of the lake. These data, taken at various subdaily intervals, were averaged over the day to provide suitable input for model simulations. The data included air temperature, relative humidity, wind speed, total daily shortwave radiation, precipitation, snowfall, and cloud cover (cloud cover measurement began in 2002 at the airport). Total precipitation is the sum of direct precipitation and conversion of snowfall to water. During a period when the cloud cover was not measured (i.e., 1989–2001), cloud cover (as a proxy for longwave radiation; Imberger and Patterson 1981) was derived from shortwave radiation based on an empirical relationship. This relationship involved fitting sinusoidal envelopes over the year to both extreme low (complete cloud cover) and extreme high (no cloud cover) values of shortwave radiation. By comparing the measured shortwave radiation on any given day to the envelope predictions, and assuming that shortwave radiation decreased linearly between the upper and lower cloud cover envelopes, we thereby estimated the daily cloud cover, with exceptional low values truncated to 100% cloud cover.

Analysis

Interannual and long-term variations in water temperature of Crystal Lake were examined using a

volumetrically weighted mean for each sample day, T_{ave}, determined as:

$$T_{ave} = \frac{\sum T_i(V_i - V_{i-1})}{\sum V_i - V_{i-1}}, \quad (16)$$

where T_i is the measured water temperature taken in the center (deepest part) of the lake at depth i, and V_i and V_{i-1} are the cumulative water volumes beneath depths i and $i - 1$, respectively. Values of T_{ave} were represented as points for water column temperature profiles taken routinely from 1981 to 2011 (Fig. 4). The continuous line ($T_{ave,mean}$) was repeated annually to show a mean value of T_{ave} for each day of the year based on the 1981–2012 profiles and using linear interpolation to generate data artificially for each day between successive measurements. A regression of $T_{ave} - T_{ave,mean}$ versus time of year (for 1981–2012) showed a positive slope (0.013; i.e., increasing T_m), although this relationship was not significant at $p < 0.05$. Variations were noted between years, however, and T_{ave} in 1992–1997, for example, tended to be consistently lower than $T_{ave,mean}$, particularly when compared with the adjacent 2–3 years (Fig. 4). Temperature profiles were not generally made at the time of ice-on or ice-off, although 4 profiles were within 3 d of ice-on, yielding a mean value of T_{ave} = 3.30 (SD 0.41) °C.

Climate change simulations

A regional climate projection downscaling from the ensemble output of 14 different GCMs at a 0.1° latitude × 0.1° longitude grid resolution was used for projections of climate change for Crystal Lake (WICCI). We obtained the projected monthly mean increase in air temperature from 1980 to 2055 for the intermediate greenhouse emission scenario (A1B) based on the latitude and longitude of Crystal Lake. The increase in annual air temperature for the study lake was found to be 3.6 °C for the A1B scenario. To address the role of groundwater flow in the future climate, we performed a sensitivity analysis by increasing and decreasing groundwater flow by 10%. Simulations of water temperature, ice phenology and thickness, and water level based on measured meteorological data ("base case") were then compared against outputs from the climate change simulations for equivalent seasons.

Results

Heat budget

Individual components of the daily surface heat budget were derived as outputs from the DYRESM-WQ-I model based on meteorological input data and the predicted surface water temperature, which was then used to calculate longwave emission and conductive and latent heat transfers. Daily inputs of shortwave radiation for 1990 (Fig. 5) were, as expected, highly variable because of daily fluctuations in cloud cover, seasonal variations in radiation, and reduced penetration of radiation during ice cover. The net longwave radiation was clearly the dominant component of the heat budget in winter. The annual maximum net heat flux occurred a few days after ice-off (also shown in other simulation years), and its occurrence was mainly due to the relatively large temperature difference between the air and surface water, resulting in greater conductive heat flux.

Water temperature

Simulated water temperatures agreed well with measurements (Fig. 6). The simulations captured observed interannual variations in temperature, such as the relatively high surface mixed layer (SML) temperatures that occurred in summers 1995 and 2002, cooler surface water temperature in the early stage of the stratified period in 1992, as well as variations occurring within

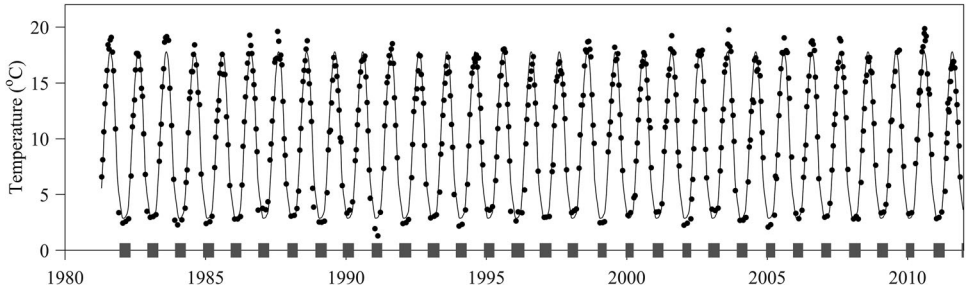

Figure 4. Volumetrically averaged temperature (T_{ave}) for Crystal Lake for each sample day (points), 1981 to 2012. The continuous line is repeated annually and shows a mean value of T_{ave} for each day of the year during 1981–2012, derived from linear interpolation between successive measurements. The repeated shaded area on the horizontal axis represents the measured duration of ice cover in each season.

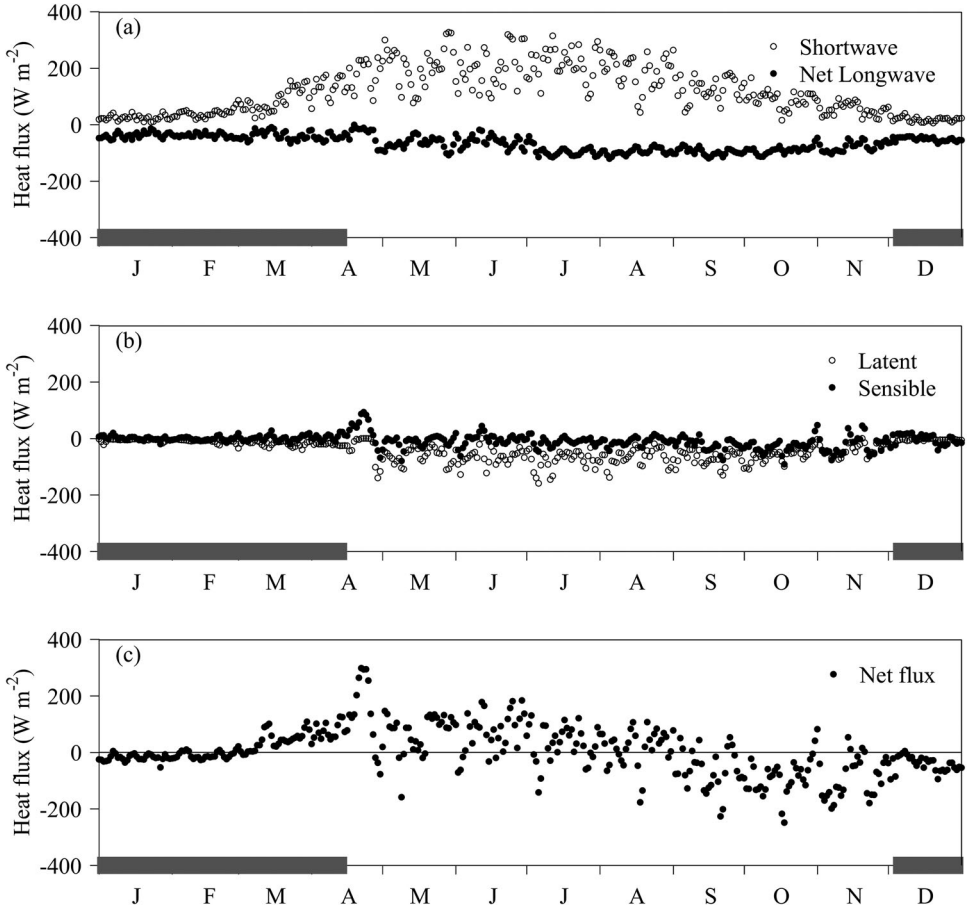

Figure 5. Heat fluxes in Crystal Lake for 1990. (a) Shortwave and net longwave fluxes, (b) latent and sensible fluxes, (c) net heat flux. The shaded area on the lower horizontal axis represents the measured duration of ice cover. The solid line in (c) denotes the zero value.

seasons, as illustrated by the 2–3 °C variations that occurred in the mixed layer during summer 1989. The differences in water column temperature (δT) between the simulation and measurements from 1989 to 2011 (Fig. 6c) show that the mean variation in temperature between the point measurements and the simulation was 0.93 °C (0.7 °C standard error [SE], $n = 8589$), close to the mean difference in T_{ave} between measurements and simulations ($\delta T = 0.5$ [0.38] °C, $n = 547$).

To further examine details of variations in water temperature beneath ice cover, we altered the scale to 0–5 °C (Fig. 6) and zoomed in on the measured and simulated data from 1989 to 1994 (Fig. 7). The adjusted scale emphasized deviations between measured data and simulation output. Direct comparison for one winter, 1990–1991 (Fig. 8), displays the difference between measured and simulated data before and under ice cover. Results show that before and immediately after ice-on, the simulation water temperatures matched well with measured values, but the errors slightly increased during February. By late March, however, the simulation predicted lower temperatures than observed. Overall, the simulations compared well with the measurements. The simulated volumetrically averaged water temperature (T_{ave}) at ice-on varied from 1.50 to 3.16 °C (mean = 2.33 °C). Simulated T_{ave} at ice-off is both warmer (mean = 4.42 °C) and more variable (range 2.75–5.10 °C), particularly compared to the variation in temperature at the bottom of the lake (3.25 to 4.44 °C) at ice-off.

Sediment heat flux

The contribution to the model compared to the previous model is the inclusion of time-varying sediment heat flux component. Observed and simulated water temperatures for 3 cases were considered (Fig. 8): time varying sediment heat flux as described in the methods section, constant sediment heat flux as in Rogers et al. (1995), and no sediment heat flux. For the case of constant sediment heat flux, we used a heat transfer rate of 2.8 W m^{-2}, as in Rogers et al. (1995). Results show that under ice cover conditions, variable sediment heat flux more closely recreates the thermal profile across all lake depths than constant heat flux or no sediment heat flux. Before and immediately following ice-on, sediment heat flux does

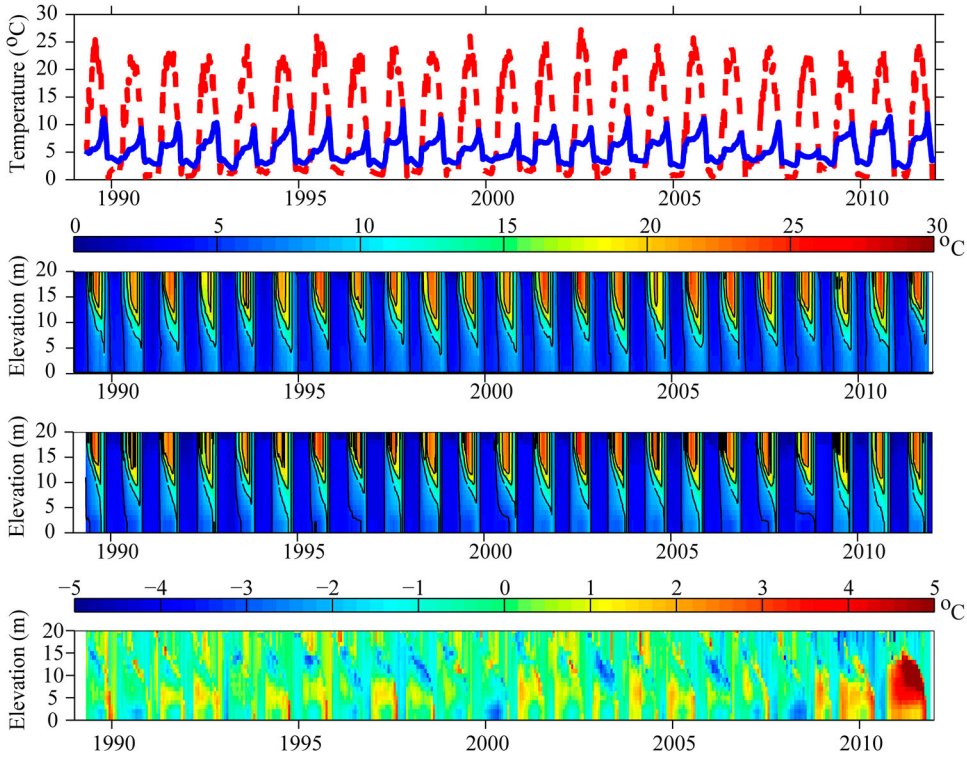

Figure 6. (a) Simulated surface water temperature (dashed red line) and bottom water temperature (solid blue line) on Crystal Lake from 2 May 1989 through 31 December 2011; (b) measurements; and (c) simulations of temperature in Crystal Lake during the same period (contour interval is 5 °C); and (d) difference between simulated and measured temperature for each measured value ($n = 8589$).

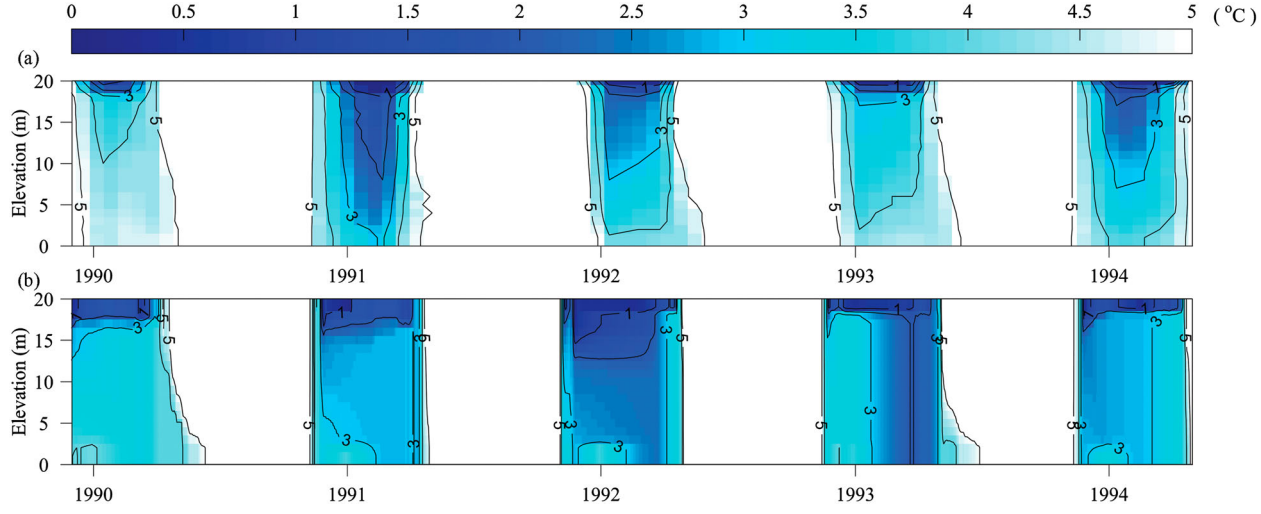

Figure 7. (a) Measured and (b) simulated temperatures in Crystal Lake for 1989–1994, with color scale representing 0–5 °C. Regions in white are >5 °C. The contour interval is 1 °C.

not significantly affect the thermal profile. In January and February, constant sediment heat flux overpredicted water temperatures at both lower and upper water depths, whereas in March, constant heat flux underpredicted water temperatures throughout the water column, illustrating the importance of time-varying sediment heat fluxes under ice cover.

Ice and snow cover

We summarized the comparison of the timing of ice-on and ice-off as well as monthly ice and snow thickness measurements (Table 3) and compared measured and simulated variations in thickness of blue ice, snow ice, and total ice (blue ice + snow ice), and snow cover (Fig. 9).

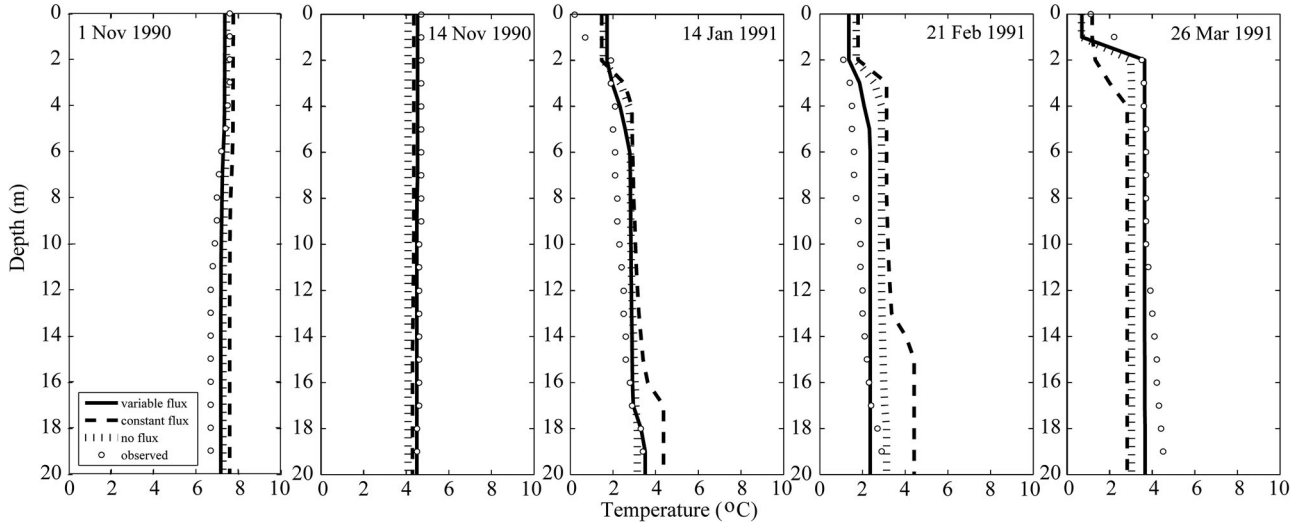

Figure 8. Observed (open circles) and simulated (solid lines) water temperatures during winter 1990–1991.

Note that the model was not calibrated to observed values for water temperature and ice cover thickness but adjusted the unmeasured groundwater inflow and outflow to match simulated lake water levels with those of observed values during the study period. The model simulations of total ice thickness were in close agreement, with <10~20% difference and a mean absolute difference of 9 (SE 0.3) cm, $n = 63$ (Fig. 9c). The model slightly overpredicted blue ice thickness and underpredicted snow ice thickness. In summary, DYRESM-WQ-I provided accurate simulations of phenological characteristics of the ice. Additionally, the measured and simulated ice duration at extended time scales (Fig. 10) indicate the model reliably captured the interannual variation of ice duration, and the results agreed closely with the measurements, except the extreme winter 1999–2000, which had the shortest ice cover duration in the past 22 years.

Sensitivity to climate change

A total ice thickness (Fig. 11) comparison of the simulations of base case and A1B scenario during 1989–2011 indicated that the A1B scenario would have thinner ice than the current base case (~0.18 m on average) and a strong interannual variation in ice cover. At the time of ice-off simulated in the A1B scenario, the base case showed up to 0.5 m of ice remaining. Ice-on date was on average 10.4 d later in the A1B scenario than in the base case, and ice-off date was 19.5 d earlier (Table 3). The resultant reductions in ice duration were well outside the range of error observed in the base case simulation for 1989–2011.

For the water budget, marked changes in water level occurred between the base case and the climate change scenarios A1B, A1B (+10% groundwater), and A1B (−10% groundwater). Over the 23-year simulation period, water levels declined to 5.1, 5.9, and 4.0 m lower than the base case for the A1B, A1B (+10% groundwater), and A1B (−10% groundwater) scenarios, respectively (Fig. 12). These changes reflect the increase in evaporation resulting from the increase in surface water temperatures in the future climate scenarios and were in marked contrast to the reproduction of observed water levels in the base case. Through the sensitivity test, we found that the effects of decreasing the groundwater flow by 10% in

Table 3. Timing and thickness of blue ice, snow ice, and snow cover in Crystal Lake based on measurements and (base) simulations from 2 May 1989 to 31 December 2011. Base and future scenarios are results from DYRESM-WQ-I simulations using observed climatic conditions (base case) and adjusted air temperatures according to the respective GCMs that reflect doubling of atmospheric CO_2. "Difference" represents departure of simulation results from measurements (for blue ice, snow ice, snow cover, and timing of base case ice-on and ice-off) or differences in timing of ice cover between base and future climate simulations using DYRESM-WQ.

Variable	Measured		Simulated		Difference		
(unit, sample size)	Mean	Range	Mean	Range	Mean	SE	Range
Blue ice (m, $n = 63$)	0.29	0.09~0.61	0.35	0.14~0.49	0.05	0.014	−0.23~0.32
Snow ice (m, $n = 63$)	0.11	0~0.43	0.07	0~0.30	−0.031	0.013	−0.32~0.18
Snow (m, $n = 63$)	0.11	0~0.46	0.10	0~0.27	−0.004	0.009	−0.28~0.16
Ice-on (d, $n = 22$), base	3 Dec	21 Nov~25 Dec	2 Dec	22 Nov~18 Dec	−1.1	0.90	−8~10
Ice-off (d, $n = 22$), base	18 Apr	28 Mar~11 May	20 Apr	4 Apr~6 May	1.4	1.55	−9~22
Ice-on (d, $n = 22$), A1B			12 Dec	28 Nov~27 Dec	10.4	1.25	4~24
Ice-off (d, $n = 22$), A1B			31 Mar	8 Mar~20 Apr	−19.5	2.44	−6 ~ −45

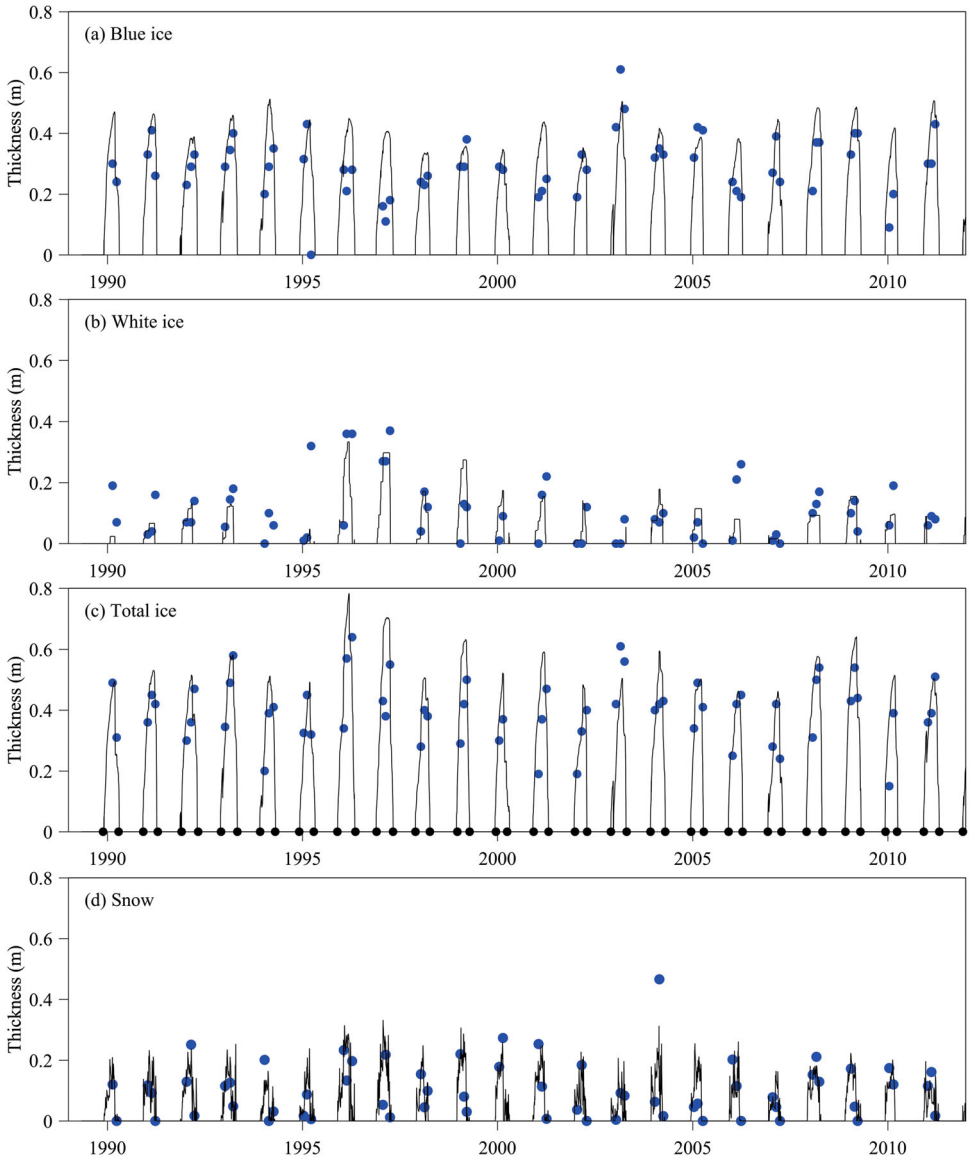

Figure 9. Measurements (circles) and simulations (lines) of blue ice, snow ice, total ice (blue ice + snow ice) and snow depth for Crystal Lake from 2 May 1989 to 31 December 2011. The dark circles in (c) denote the ice-on and ice-out dates in each season.

Crystal Lake (net groundwater flow is out of the lake) was equivalent to 21% of the reduction in water level.

Extending the simulation run continuously into a second season of summer stratification allowed the effect of an identical initial temperature profile for the 2 simulations to be negated. A consistently higher temperature in the hypolimnion of the A1B scenario was observed in the second summer (Fig. 13). Comparisons

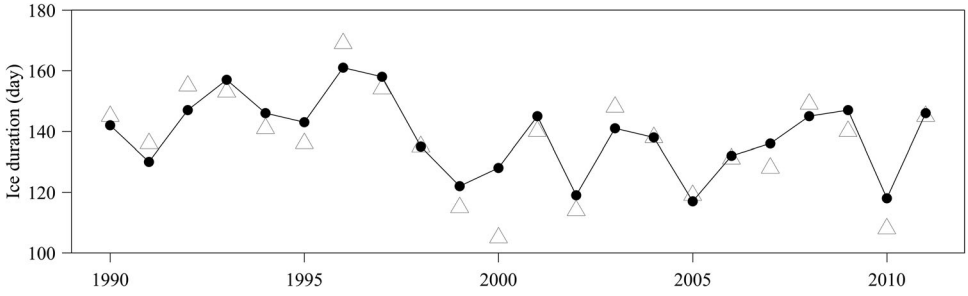

Figure 10. Measurements and simulations (continuous line intersecting filled circles) of ice duration for Crystal Lake during 1989–2011.

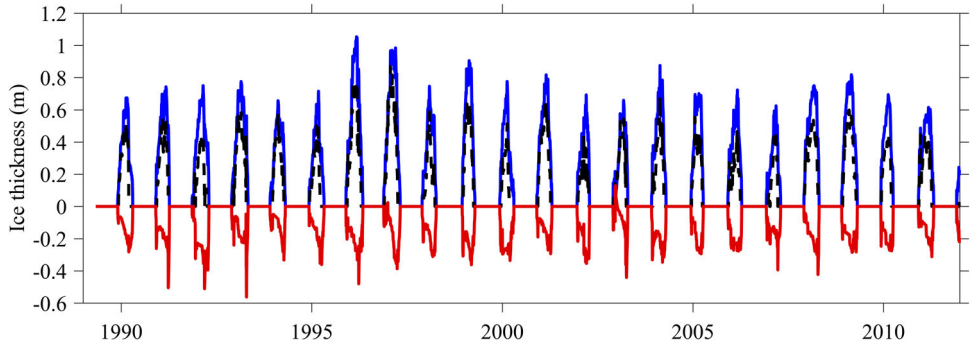

Figure 11. Simulated total ice thickness (positive values) for base case (solid lines) and the A1B scenario (dark dashed lines). The negative values represent the decrease in thickness in the A1B scenario relative to the base case

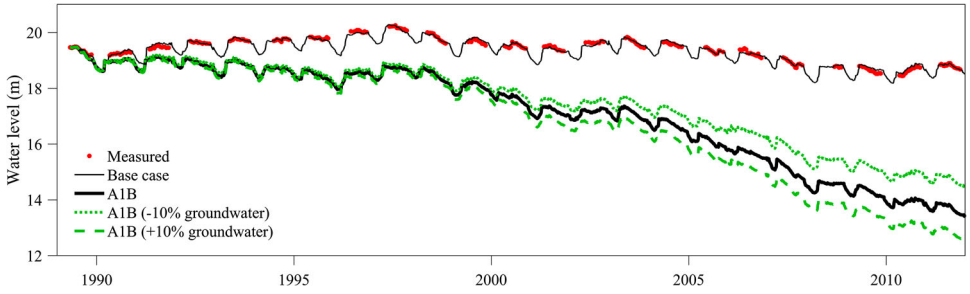

Figure 12. Measured and simulated water levels in Crystal Lake from 2 May 1989 to 31 December 2011.

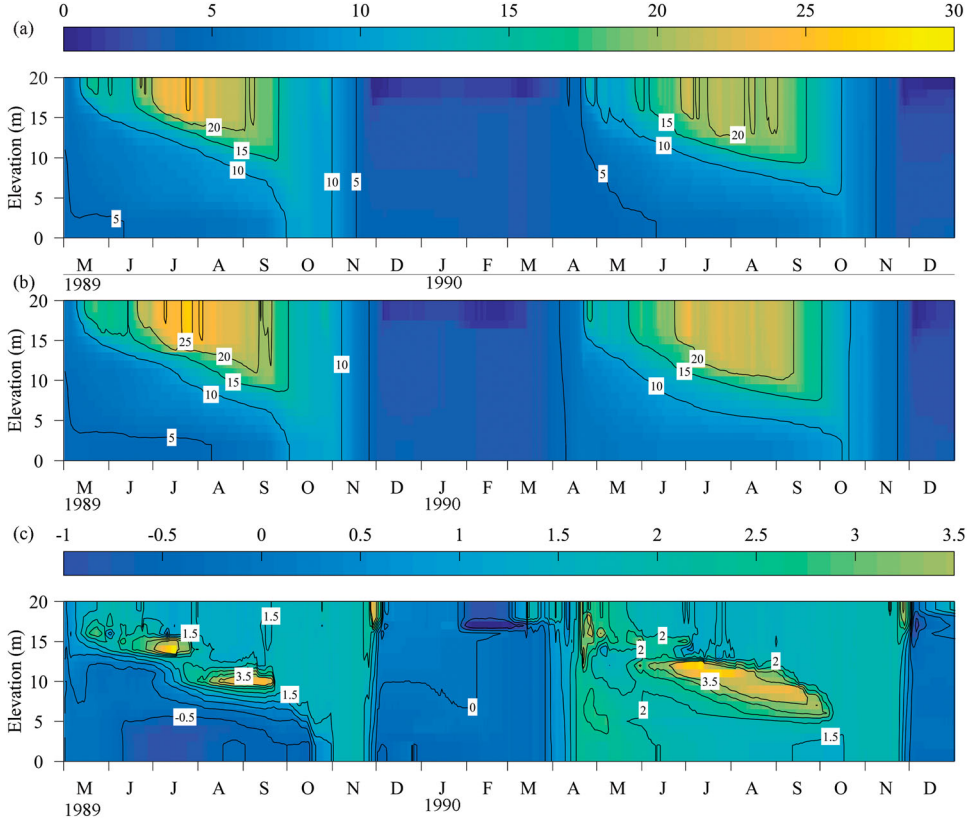

Figure 13. Water temperature in the (a) current and (b) future climate A1B scenario for simulations from 2 May 1989 to 31 December 1990, and (c) change in temperature in the future climate A1B scenario relative to the base case for the same period.

of temperature between the base case and the A1B scenario showed marked variations, both temporally and spatially. Open-water conditions were characterized by increases in water temperature of ~1–3.5 °C in the SML for the A1B scenario. These increases were accentuated at mid-depth, particularly in the second season when the SML was substantially deeper in the A1B scenario. The characteristic deepening of the SML in the first summer was not repeated in the second, and the differences remain relatively constant through depth during the second season. Temperature in the hypolimnion in the first summer was mostly indicative of the initial profile and isolation of this region from surface fluxes during presence of strong stratification, which was enhanced slightly by increased temperature in the surface layer. As a result, a slight decrease in water temperature occurred in the hypolimnion in the A1B scenario. This trend was reversed in the second summer, however, when at the onset of stratification temperature in the A1B scenario was elevated considerably over the base case. In winter, differences were reduced and generally reversed, when a ~0 to −1 °C difference characterized much of the water column.

Discussion

Water temperature modeling

The difference between the simulation results and observations was acceptable, with the largest consistent deviations in δT (3.2 °C) occurring in the thermocline region over summer and smaller deviations occurring in the SML and bottom waters. Standard errors (SE 0.7 °C) using the DYRESM-WQ-I model compared well with those of other studies including the Hostetler model (RMSE = 2 °C; Hostetler and Bartlein 1990) and Minlake model (SE 1.07 °C for the total simulation period; Fang and Stefan 1996a). Compared to observations, simulations produced a slight mismatch in thermocline depths and the timing of stratification onset and overturn in some years. The temperature in the lower water column during fall mixing tended to be warmer than observations owing to the earlier fall mixing simulated in the model. Adjustments to mixing parameters used in DYRESM-WQ were previously shown to reproduce measured data with greater accuracy (e.g., Jellison et al. 1998). In this case, our inability to differentiate inaccuracies in model input data (e.g., local wind speeds) from inadequate model process representations would effectively mean that improvements in δT would not necessarily be related to meaningful process adjustments. Furthermore, while the use of 1D modeling in this study is justified based on detailed field measurements (Bengtsson et al. 1996), the inherently 3D nature of transport processes beneath ice, particularly in relation to groundwater and sediment-water heat exchanges, should not be neglected. Specifically, the existence of bottom currents toward deeper regions of ice-covered lakes (e.g., Likens and Ragotzkie 1965) may occur through advective transport of relatively warm (or solute-enriched) waters from groundwater intrusions closer to the water surface and conductive and/or porewater exchanges along the lakebed.

Water temperature under ice

Both measured and simulated data showed a buildup of relatively warm (~4 °C) water in the lower part of the water column during each period of ice cover except for 1993. The increase in temperature of the bottom water to >4 °C in late winter produced a brief period of complete water column mixing except for a layer of cool water ~1 m below the ice. This event occurred immediately before the period of vertically oriented 4 °C isotherms. This feature was not evident in the measured data collected in Crystal Lake because of limited sampling frequency throughout the ice-covered period in each season, but it was observed in Sparkling Lake (located 7 km west of Crystal Lake) during 2001–2005 when the water temperature under the ice cover was collected at higher frequency (hourly) than in the other lakes (Malm et al. 1997, Zdorovennova 2009). The near-complete winter mixing prior to ice-off may have important biogeochemical effects that may exert short-term rather than progressive stress on organisms, potentially negating adaptive responses. For example, this period can be critical for winter fish habitat if unoxidized organic matter in deeper, anoxic waters is redistributed through all but the thin surface layer adjacent to ice. The potential then exists for widespread (water column) oxygen depletion when reaeration is restricted by ice cover, and temperature in near-surface waters may be too cold to provide suitable fish habitat.

Ice–snow modeling

Simulated ice and snow thickness match well with observed values, with largest differences in snow thickness over ice. Minlake (Fang and Stefan 1996a) had similar but slightly higher errors for ice thickness (11 cm), as found in this study, as did LIMNOS for ice dates (Vavrus et al. 1996). A recent study by Magee and Wu (2017a) reported a similar range of simulated ice and snow thickness for 3 southern lakes in Wisconsin. Errors in ice and snow cover thickness likely play a role in errors of under-ice water temperatures, especially during January and

February. One potential reason for the discrepancy in snow cover and snow ice thickness between simulated results and observations (Fig. 8 and 9) is the nonuniform distribution of snow accumulation. Liston and Hall (1995) indicated that both the wind speed and direction can affect snow accumulation, which is important for ice growth through thermal and snow ice formation mechanisms. Bengtsson (1986) showed high spatial variations in ice and snow depths for lakes similar in size to Crystal Lake. Previous research has stressed the importance of accurately simulating ice cover when determining under-ice water temperatures and circulation patterns (Kirillin et al. 2012, Yang et al. 2012, Oveisy and Boegman 2014). In mid-latitude lakes, variability of snow and ice albedo are critical to appropriately capture the penetration of shortwave solar radiation through ice and into the water column (Vavrus et al. 1996, Kirillin et al. 2012, Yang et al. 2012). Additionally, a white-ice component of the model is necessary because it could form as much as 16% of total ice thickness during the winter in some lakes (Yang et al. 2012), and properties of white-ice cover differ from those of blue-ice cover (Rogers et al. 1995), affecting heat fluxes to the water column (Kirillin et al. 2012, Yang et al. 2012). Overall, the advantage of including ice and snow dynamics in the hydrodynamic model in this study indicates that simulations can be run for multiple years with the potential to uncover phenomena not apparent in shorter or discontinuous simulations. In our continuous simulations, an increase in hypolimnion temperature in the second year contrasted with a slight decrease in the first year in the GCM scenarios relative to the base case. Peeters et al. (2002) suggest that the presence of ice cover in dimictic lakes may make it acceptable to use a discontinuous simulation approach, neglecting heat carryover from year to year. Our continuous simulations of GCM scenarios, however, indicate that previously simulated decreases in hypolimnion temperature with climate warming (e.g., De Stasio et al. 1996) may be an artifact of this discontinuous simulation approach.

Thermal regime and ice phenology in response to the projected climate

Simulations based on the future climate A1B scenarios show substantial differences from the base case. The large difference in temperature in the hypolimnion between the 2 summers of our future climate simulation (Fig. 13) reinforces conclusions drawn from other studies (e.g., Robertson and Ragotzkie 1990) that depth and duration of summer stratification are highly dependent on spring conditions when thermal stratification develops. In the second summer stratification period of the future climate simulation (A1B), the volume of the hypolimnion was reduced substantially relative to that in the base case, and therefore the sediment surface area to hypolimnetic water volume ratio would increase. This change, together with increased duration of stratification, suggests an increased likelihood of summer anoxia in hypolimnetic waters. Similar conclusions have been made in other studies (e.g., De Stasio et al. 1996, Stefan et al. 1998, Fang and Stefan 2009), but resultant impacts on summer phytoplankton biomass may be complicated by complex interactions among physical and biogeochemical factors. For example, increased duration of anoxia and remobilization of nutrients from sediments in the hypolimnion can act to enhance phytoplankton production. Conversely, increased strength and duration of stratification, greater sedimentation and SML depth, and associated reduction in mean SML light levels would have the reverse effect. Conditions under future climate scenarios generally seem more conducive to proliferation of bloom-forming algae (e.g., cyanobacteria; Lathrop et al. 1999). These conditions include reduced turbulence, warmer SML temperature, increased stratification, and greater sedimentation losses of nutrients from the SML. Specific adaptations of cyanobacteria, such as high Q_{10} for growth (Reynolds 1997), buoyancy regulation (Wallace and Hamilton 1999), and potential to fix nitrogen in some species (Oliver and Ganf 2000) may be especially advantageous under these conditions (see Paerl and Huisman 2008).

An important outcome from this study is that for future climate scenarios, compensatory changes in heat fluxes (other than conductive heat exchange) or hydrology are required to maintain present water levels in Crystal Lake. Latent heat exchange will undoubtedly favor heat loss from the water surface, but this process was incorporated in the model and is therefore accounted for in the future climate simulations. Changes in other heat fluxes, particularly shortwave and longwave radiation, as well as wind may occur with projected global warming scenarios, but the direction and magnitude of these fluxes are still somewhat uncertain (IPCC 2013) and at times could even be counter directional to changes from increasing air temperature (Tanentzap et al. 2008). Direct contributions to the water balance by components other than evaporation remain the most likely mechanism to alter projected decreases in water level. GCM rainfall projections suggest an annual increase of 4.8% for the A1B climate scenario (downscaled over WI, USA), representing variations from 38.1 mm based on annual mean rainfall (1989–2011) for Crystal Lake of 800 mm. Changes of this magnitude or other observed long-term changes in precipitation in the region (+2.4% per decade; Magnuson et al. 1997) may not compensate for

the projected decreases in water level of +175 and +260 mm yr^{-1} under the A1B future climate scenario with −10% and +10% groundwater input, respectively. Previous studies indicate that surface runoff into the lake is negligible, and that most of the water budget (~95%) is dominated by direct precipitation and evaporation from the lake surface (Kenoyer and Anderson 1989, Anderson and Cheng 1993), so precipitation-generated runoff may not be sufficient to compensate for increases in evaporation over the lake surface. Additional studies linking surface runoff and groundwater inflow to the lake hydrodynamic model may be required to fully assess the response of lake ecosystem to climate changes.

Conclusions

We continuously simulated the ice phenology and water temperature of Crystal Lake from 2 May 1989 to 31 December 2011 without interruption to investigate the effects of changing air temperatures on a northern Wisconsin dimictic lake. Downscaled regional future climate projections based on the intermediate greenhouse emissions scenario (A1B) for the mid-21st century from WICCI were used to run future climate scenarios on Crystal Lake using the DYRESM-WQ-I model. The average reduction in mean total ice thickness was found to be ~18 cm. The surface mixed-layer temperature increased by up to 3.5 °C over summer, and the increased evaporation may cause large water level declines. The decline in water level resulting from the increased surface water temperature and evaporation may potentially be the most important effect of climate warming on this small seepage lake. Most reporting of climate change effects on lakes has focused on the effect of decreases in ice duration, increases in SML layer depth and temperature, and resultant impacts on the biota, but we suggest that hydrological factors must now be integrated much more closely into these assessments.

Acknowledgements

Data for the model were compiled from the North Temperate Lakes Long-Term Ecological Research Project database. The project is funded by the US National Science Foundation Long-Term Ecological Research Program and University of Wisconsin Water Resources Institute USGS 104(B) Research Grant Project and the University of Western Australia Gledden Study Leave Award. We especially thank Yi-Fang Hsieh, Brett Wallace, and John Patterson for assistance with development of the ice model, and John Magnuson and the late Tom Frost of the Center for Limnology for their support and valuable discussions and comments during the early preparation of this manuscript. Paulette Homant from the Wisconsin Department of Natural Resources who provided information on groundwater characteristics of Crystal Lake is also acknowledged. We thank the Associate Editor and 2 anonymous reviewers for providing helpful comments to greatly improve the quality of this paper.

ORCID

David P. Hamilton http://orcid.org/0000-0002-9341-8777
Madeline R. Magee http://orcid.org/0000-0002-2741-2262
Chin H. Wu http://orcid.org/0000-0001-8393-1940

References

Agbeti MD, Smol JP. 1995. Winter limnology: a comparison of physical, chemical and biological characteristics in two temperate lakes during ice cover. Hydrobiologia. 304:221–234.

Anderson MP, Cheng X. 1993. Long- and short-term transience in a groundwater/lake system in Wisconsin, USA. J Hydrol. 145:1–18.

Ashton GD. 1986. River and lake ice engineering. Littleton (CO): Water Resources Publications.

Assel RA, Robertson DM. 1995. Changes in winter air temperatures near Lake Michigan, 1851–1993, as determined from regional lake-ice records. Limnol Oceanogr. 40:165–176.

Bengtsson L. 1986. Spatial variability of lake ice covers. Geogr Ann. 68A:113–121.

Bengtsson L, Malm J, Terzhevik A, Petrov M, Boyarinov P, Glinsky A, Palshin N. 1996. Field investigation of winter thermo- and hydrodynamics in a small Karelian lake. Limnol Oceanogr. 41:1502–1513.

Birge EA, Juday C, March HW. 1927. The temperature of the bottom deposits of Lake Mendota; a chapter in the heat exchanges of the lake. T Wisc Acad Sci Arts Lett. 23:187–231.

Bueche T, Hamilton DP, Vetter M. 2017. Using the General Lake Model (GLM) to simulate water temperatures and ice cover of a medium-sized lake: a case study of Lake Ammersee, Germany. Environ Earth Sci. 76:461.

Carpenter SR, Fisher SG, Grimm NB, Kitchell JF. 1992. Global change and freshwater ecosystems. Annu Rev Ecol Syst. 23:119–139.

De Stasio BT, Hill DK, Kleinhans JM, Nibbelink NP, Magnuson JJ. 1996. Potential effects of global climate change on small north-temperate lakes: physics, fish, and plankton. Limnol Oceanogr. 41:1136–1149.

Ellis CR, Stefan HG, Gu R. 1991. Water temperature dynamics and heat transfer beneath the ice cover of a lake. Limnol Oceanogr. 36:324–335.

Fang X, Ellis CR, Stefan HG. 1996. Simulation and observation of ice formation (freeze-over) in a lake. Cold Reg Sci Technol. 24:129–145.

Fang X, Stefan HG. 1996a. Long-term lake water temperature and ice cover simulations/measurements. Cold Reg Sci Technol. 24:289–304.

Fang X, Stefan HG. 1996b. Dynamics of heat exchange between sediment and water in a lake. Water Resour Res. 32:1719–1727.

Fang X, Stefan HG. 2009. Simulations of climate effects on water temperature, dissolved oxygen, and ice and snow covers in lakes of the contiguous U.S. under past and future climate scenarios. Limnol Oceanogr. 54:2359–2370.

Gill AE. 1982. Atmosphere–ocean dynamics. Cambridge (MA): Academic Press.
Gu R, Stefan HG. 1990. Year-round temperature simulation of cold climate lakes. Cold Reg Sci Technol. 18:147–160.
Hamilton DP, Schladow SG. 1997. Prediction of water quality in lakes and reservoirs: Part I - Model calibration, sensitivity analysis and application. Ecol Model. 96:91–110.
Harvey LDD. 1990. Testing alternative parameterizations of lateral melting and upward basal heat flux in a thermodynamic sea ice model. J Geophys Res-Oceans. 95:7359–7365.
Hill JM, Kucera A. 1983. Freezing a saturated liquid inside a sphere. Int J Heat Mass Trans. 26:1631–1637.
Hostetler SW, Bartlein PJ. 1990. Simulation of lake evaporation with application to modeling lake level variations of Harney-Malheur Lake, Oregon. Water Resour Res. 26:2603–2612.
Hutchinson GE. 1975. A treatise on limnology, Vol. 1: Geography and physics of lakes. New York (NY): John Wiley & Sons.
Imberger J, Patterson JC. 1981. Dynamic reservoir simulation model - DYRESM: 5. In: Fischer HB, editor. Transport models for inland and coastal waters. Cambridge (MA): Academic Press; p. 310–361.
Imberger J, Patterson JC. 1990. Physical limnology. Adv Appl Mech. 27:303–475.
[IPCC] Intergovernmental Panel on Climate Change. 2013. Summary for policymakers. In: Stocker T, Qin D, Plattner G-K, Tignor M, Allen SK, Boschung J, Nauels A, Xia Y, Bex V, Midgley PM, editors. Climate change 2013: the physical science basis. Contribution of Working Group I to the Fifth Assessment Report of the Intergovernmental Panel on Climate Change. New York (NY): Cambridge University Press.
Jellison R, Romero J, Melack JM. 1998. The onset of meromixis during restoration of Mono Lake, California: unintended consequences of reducing water diversions. Limnol Oceanogr. 43:706–711.
Jensen OP, Benson BJ, Magnuson JJ, Card VM, Futter MN, Soranno PA, Stewart KM. 2007. Spatial analysis of ice phenology trends across the Laurentian Great Lakes region during a recent warming period. Limnol Oceanogr. 52:2013–2026.
Kenoyer GJ, Anderson MP. 1989. Groundwater's dynamic role in regulating acidity and chemistry in a precipitation-dominated lake. J Hydrol. 109:287–306.
Kirillin G, Leppäranta M, Terzhevik A, Granin N, Bernhardt J, Engelhardt C, Efremova T, Golosov S, Palshin N, Sherstyankin P, et al. 2012. Physics of seasonally ice-covered lakes: a review. Aquat Sci. 74:659–682.
Kucharik CJ, Serbin SP, Vavrus S, Hopkins EJ, Motew MM. 2010. Patterns of climate change across Wisconsin from 1950 to 2006. Phys Geogr. 31:1–28.
Lathrop RC, Carpenter SR, Robertson DM. 1999. Summer water clarity responses to phosphorus, Daphnia grazing, and internal mixing in Lake Mendota. Limnol Oceanogr. 44:137–146.
Likens GE, Ragotzkie RA. 1965. Vertical water motions in a small ice-covered lake. J Geophys Res. 70:2333–2344.
Liston G, Hall DK. 1995. An energy balance of lake-ice evolution. J Glaciol. 41:373–382.
Magee M, Wu CH, Robertson DM, Lathrop RC, Hamilton DP. 2016. Trends and abrupt changes in 104-years of ice cover and water temperature in a dimictic lake in response to air temperature, wind speed, and water clarity drivers. Hydrol Earth Syst Sc. 20:1681–1702.
Magee M, Wu CH. 2017a. Long-term trends and variability of ice cover in three morphometrically different lakes in response to climate change. Hydrol Proc. 31:308–323.
Magee M, Wu CH. 2017b. Response of water temperatures and stratification to changing climate in three lakes with different morphometry. Hydrol Earth Syst Sc. 21:6253–6274.
Magnuson JJ, Kratz TK, Benson BJ. 2006. Long-term dynamics of lakes in the landscape: long-term ecological research on north temperate lakes. Berlin (Germany) and New York (NY): Oxford University Press.
Magnuson JJ, Webster KE, Assel RA, Bowser CJ, Dillon PJ, Eaton JG, Evans HE, Fee EJ, Hall RI, Mortsch LR, et al. 1997. Potential effects of climate changes on aquatic systems: Laurentian Great Lakes and Precambrian Shield Region. Hydrol Proc. 11:825–871.
Malm J, Terzhevik A, Bengtsson L, Boyarinov P, Glinsky A, Palshin N, Petrov M. 1997. Temperature and salt content regimes in three shallow ice-covered lakes. 1. Temperature, salt content, and density structure. Nord Hydrol. 28:99–128.
Maykut GA. 1982. Large-scale heat exchange and ice production in the central arctic. J Geophys Res. 87:7971–7984.
Maykut GA, Untersteiner N. 1971. Some results from a time-dependent thermodynamic model of sea ice. J Geophys Res. 76:1550–1575.
McKay G. 1968. Problems of measuring and evaluating snow cover. In: Proceedings Workshop Seminar of Snow Hydrology, Ottawa, Canada; p. 49–63.
Melack JM, Dozier J, Goldman CR, Greenland D, Milner AM, Naiman RJ. 1997. Effects of climate change on inland waters of the Pacific coastal mountains and Western Great Basin of North America. Hydrol Proc. 11:971–992.
Oliver R, Granf G. 2000. Freshwater blooms. In: Whitton B, Potts M, editors. The ecology of Cyanobacteria. Amsterdam (Netherlands): Kluwer; p. 149–194.
Oveisy A, Boegman L. 2014. One-dimensional simulation of lake and ice dynamics during winter. J Limnol. 73:441–453.
Paerl HW, Huisman J. 2008. Blooms like it hot. Science. 320:57–58.
Patterson JC, Hamblin PF. 1988. Thermal simulation of a lake with winter ice cover. Limnol Oceanogr. 33:323–338.
Peeters F, Livingstone DM, Goudsmit G-H, Kipfer R, Forster R. 2002. Modeling 50 years of historical temperature profiles in a large central European lake. Limnol Oceanogr. 47:186–197.
Reynolds CS. 1997. Vegetation processes in the pelagic: a model for ecosystem theory. Oldendorf (Germany): Ecology Institute.
Robertson DM, Ragotzkie RA. 1990. Changes in the thermal structure of moderate to large-sized lakes in response to changes in air temperature. Aquat Sci. 52:360–380.
Robertson DM, Ragotzkie RA, Magnuson JJ. 1992. Lake ice records used to detect historical and future climatic changes. Clim Change. 21:407–427.
Rogers CK, Lawrence GA, Hamblin PF. 1995. Observations and numerical simulation of a shallow ice-covered midlatitude lake. Limnol Oceanogr. 40:374–385.
Saloranta TM, Andersen T. 2007. MyLake—a multi-year lake simulation model code suitable for uncertainty and sensitivity analysis simulations. Ecol Model. 207:45–60.

Scheller RM, Mladenoff DJ. 2005. A spatially interactive simulation of climate change, harvesting, wind, and tree species migration and projected changes to forest composition and biomass in northern Wisconsin, USA. Glob Change Biol. 11:307–321.

Schindler DW, Bayley SE, Curtis PJ, Parker BR, Stainton MP, Kelly CA. 1992. Natural and man-caused factors affecting the abundance and cycling of dissolved organic substances in precambrian shield lakes. Hydrobiologia. 229:1–21.

Scott J. 1964. A comparison of the heat balance of lakes in winter [dissertation]. Madison (WI): University of Wisconsin-Madison.

Serbin SP, Kucharik CJ. 2009. Spatiotemporal mapping of temperature and precipitation for the development of a multidecadal climatic dataset for Wisconsin. J Appl Meteorol Clim. 48:742–757.

Stefan HG, Fang X, Hondzo M. 1998. Simulated climate change effects on year-round water temperatures in temperate zone lakes. Climatic Change. 40:547–576.

Stefan HG, Hondzo M, Fang X, Eaton JG, McCormick JH. 1996. Simulated long term temperature and dissolved oxygen characteristics of lakes in the north-central United States and associated fish habitat limits. Limnol Oceanogr. 41:1124–1135.

Tanentzap AJ, Norman DY, Keller B, Girard R, Heneberry J, Gunn JM, Hamilton DP, Taylor PA. 2008. Cooling lakes while the world warms: effects of forest regrowth and increased dissolved organic matter on the thermal regime of a temperate, urban lake. Limnol Oceanogr. 53:404–410.

Tsay T, Ruggaber G, Effler S, Driscoll C. 1992. Thermal stratification modeling of lakes with sediment heat flux. J Hydraul Eng. 118:407–419.

Vavrus SJ, Wynne RH, Foley JA. 1996. Measuring the sensitivity of southern Wisconsin lake ice to climate variations and lake depth using a numerical model. Limnol Oceanogr. 41:822–831.

Wallace BB, Hamilton DP. 1999. The effect of variations in irradiance on buoyancy regulation in *Microcystis aeruginosa*. Limnol Oceanogr. 44:273–281.

Webster KE, Bowser CJ, Anderson MP, Lenters JD. 2006. Understanding the lake-groundwater system: just follow the water. In: Magnuson JJ, Kratz TK, Benson B, editors. Long-term dynamics of lakes in the landscape: long-term ecological research on northern temperate lakes. Oxford (UK): Oxford University Press; p. 19–48.

Weyhenmeyer GA, Blenckner T, Pettersson K. 1999. Changes of the plankton spring outburst related to the North Atlantic Oscillation. Limnol Oceanogr. 44:1788–1792.

Yang Y, Leppäranta M, Cheng B, Li Z. 2012. Numerical modelling of snow and ice thicknesses in Lake Vanajavesi, Finland. Tellus A. 64:1.

Zdorovennova GE. 2009. Spatial and temporal variations of the water–sediment thermal structure in shallow ice-covered Lake Vendyurskoe (Northwestern Russia). Aquat Ecol. 43:629–639.